

EXTENDED EXPERIMENTAL PROCEDURES

Model Formulation

Basic Cascade (Figure 1)

Based on our experimental setup, we assumed that the kinases Raf:ER, MEK1 and ERK2 were expressed at the same concentration and allowed to reach steady-state levels before the addition of estradiol. Equilibrium was reached through the balance of synthesis and degradation terms. The degradation reactions of all forms of kinases were modeled with first-order kinetics, and the active species were assumed to degrade at the same rate as their respective inactive forms. Binding of estradiol to Raf:ER activated the Raf:ER kinase (Raf:ER*). We modeled activation of MEK1 and ERK2 via dual, nonprocessive phosphorylation events. We assumed that both phosphorylation events for a given kinase occur with the same k_{cat} and K_M . These constants were initially taken from Levchenko et al. (2000); the K_M values were subsequently refined during global fitting of the model to experimental data. Our refined K_M values (120 nM for MEK substrate and 40 nM for ERK substrate) are in close agreement with those reported in the Levchenko paper (150 nM for MEK substrate and 35 nM for ERK substrate). We simulated estradiol titration, allowed the system to reach steady state, and normalized the concentration of activated ERK2 (ERK2_{pp}) by the initial value of total ERK2.

Variable Expression (Figure 2)

For variable cascade simulations, Raf:ER was assigned the same value as in the basic cascade while the levels of MEK1 and ERK2 were varied, consistent with our experimental setup. In the variable cascade model, all parameters were identical to those in the basic cascade model, with only the MEK1 and ERK2 synthesis rates altered to vary the steady-state concentrations of these kinases.

Basic Cascade with Scaffold (Figure 3)

We assumed that MEK1 and ERK2 were in equilibrium with the scaffold before the addition of estradiol. The scaffold protein (pax*) used in our experiments has been shown to strongly localize to the sites of polarized growth in yeast (Gao et al., 2004), so we used a compartmental model of cascade activation in which scaffolded species were treated independently from those in solution. We assumed that the dissociation of scaffold-bound MEK1 and ERK2 does not lead to activation of these kinases in solution due to diffusion limitation. Further, when bound on the same scaffold molecule, MEK1 activates ERK2 in a processive manner. The degradation reactions of scaffold and all scaffold-bound species were also modeled with first-order kinetics. The compartmental model was simulated for low and high levels of scaffold and the total steady-state ERK2_{pp} levels (accounting for both activation in solution and scaffold-mediated activation) were compared with experiments in Figure 3.

Negative Regulation (Figure 4)

In modeling the ERK2 phosphatase (MKP1-cyt), we assumed that dephosphorylation of ERK2_{pp} occurred as a two-step (distributive) reaction. We also assumed that both dephosphorylation reactions have the same k_{cat} and K_M . The small-molecule inhibitor of MEK1 (CI-1040) was assumed to bind only to inactive MEK1 and we assumed this binding reaction was at equilibrium before the addition of estradiol. We also assumed that Raf:ER did not activate inhibitor-bound MEK1.

Basic and Variable Expression Cascades with Single-Step Phosphorylation (Figure 6)

To analyze the contribution of dual-step phosphorylation to ultrasensitivity in MAPK cascades, we remodeled the basic and variable cascades to simulate only a single (or lumped) phosphorylation step at each tier. As in the original models, binding of estradiol to Raf:ER induced its activation. Active Raf:ER induced a single phosphorylation of MEK (considered here to be an active kinase species), which in turn phosphorylated ERK once. The concentrations of the kinases and other parameters involved in their synthesis, degradation, association, dissociation and activation were identical to those in the corresponding dual-step phosphorylation models.

Hill Equations (Figure 6)

To analyze the role of cascading itself in generating ultrasensitivity, we accurately fit a Hill equation to a simulated steady-state dose-response curve from each explicit model. This Hill equation converted estradiol concentration into a total concentration of active MEK. The fitted Hill equations were then used to determine the ultrasensitivity of the dose-response relationship between estradiol and active ERK; this result was compared to the ultrasensitivity of the same dose-response curve obtained with the corresponding full model. The synthesis, degradation, association, dissociation and activation for ERK species were identical to those in the corresponding full models.

The series of ODEs for each model was solved using the numerical stiff solver ode23s in MATLAB (The Mathworks). Steady-state response plots, 3D surface plots and 2D heat maps were also generated in MATLAB.

Parameters and Initial Conditions

All parameters and initial conditions in the basic cascade were refined from literature values by globally fitting the Hill coefficient, signal strength and EC_{50} to the experimental steady-state response curves for the basic and high-MEK variable cascades (only changing MEK1 and ERK2 synthesis rates in the variable cascade). The initial conditions and common parameters were kept constant in the low-MEK variable cascade, MEK1-inhibitor, and ERK2-phosphatase models. In the scaffolding model, these parameters gave the qualitative trends that we observed experimentally, but the parameters were refit to improve resolution. Complete lists of reactions, differential equations, parameters and initial conditions for the basic cascade and other models are provided in Table S4, Table S5, Table S6, Table S7, Table S8, and Table S9.

Fluorescence Microscopy

Codon-optimized *MEK1-mCherry* and *mCherry-ERK2* were custom synthesized by Geneart. Each gene was subcloned into an integration vector under the control of P_{tetO7} and an episomal vector under the control of P_{Gal} . Transformed cells were grown from a fresh colony in SC media for 24 hr at 30°C with shaking. Cultures were diluted into fresh SC media with the appropriate inducer (0.5 µg/ml aTC or 2% galactose) and grown for 16 hr to an OD_{660} of 0.4–0.5. Cells were visualized for fluorescence with a Zeiss Axiovert 40 CFL.

Endogenous Dephosphorylation Assay

Strains were grown from a fresh colony in SC media for 24 hr with shaking at 30°C. Liquid culture was diluted 1:250 into 25 ml SC media with 2% galactose (no glucose) and 0.5 µg/ml aTC (Sigma Aldrich), and grown for 16 hr to a final OD_{660} of 0.7–0.8. Cultures were stimulated with 73.4 µM estradiol for 30 min with shaking at 30°C and were pelleted at room temperature for 3 min at 3000 × g. Cells were washed three times for 10 min each in SC media containing 2% galactose and 0.5 µg/ml aTC, with or without phosphatase inhibitors (100 µM freshly prepared pervanadate and 10 mM NaF, Sigma Aldrich). Cells were then resuspended in the appropriate media (with or without inhibitors) and incubated with shaking at 30°C for 1 hr. Aliquots were taken for lysis at 0, 20, 40 and 60 min and were lysed with the NaOH/SDS protocol described in the main text. Phosphorylated ERK levels were determined by quantitative western blotting.

Coimmunoprecipitation

Cell Growth and Lysis

Strains were grown from a fresh colony in SC media for 24 hr with shaking at 30°C. Liquid culture was diluted 1:250 into 50 ml SC media with 2% galactose (no glucose) and 0.5 µg/ml aTC (Sigma Aldrich), and grown for 20 hr to a final OD_{660} of 1.0. Cells were harvested by centrifugation at 4°C for 5 min at 1500 × g, washed once in ice-cold water and cell pellets were collected. The weight of the wet cell pellet was determined and the volume estimated by 1 g ≈ 1 ml. The cell pellet was resuspended in 3 volumes ice-cold lysis buffer (20 mM Tris-HCl, 100 mM NaCl, 300 mM ammonium sulfate, 5% glycerol, 10 mM MgCl₂, 1 mM EDTA, 1 mM DTT, 0.1% Triton-X, 1 mM PMSF, protease inhibitor cocktail (Sigma, #P8215), phosphatase inhibitor cocktails (Sigma, #P2850, #P5726)) and 4 volumes of ice-cold glass beads (Sigma, #G8772). The slurry was vortexed at maximum speed for 45 s and cooled immediately in ice water for 45 s. Cells were vortexed and cooled for 10 cycles, and the supernatant was collected. The glass beads were washed with 3 volumes lysis buffer, vortexed briefly, and the supernatant was collected and pooled. Pooled supernatants were centrifuged at 4°C for 60 min at 12,000 × g and decanted. Crude extracts were aliquoted and used directly or flash frozen at –80°C.

Coimmunoprecipitation

One mg of total protein was brought to a final volume of 500 µl and incubated with 1 µg anti-paxillin antibody (BD Biosciences) overnight at 4°C. Complexes were collected with 50 µl DYNA G beads (Invitrogen), and beads were washed three times in co-IP buffer (50 mM Tris-HCl, 100 mM NaCl, 1 mM EDTA, 0.1% Triton-X, 1 mM DTT, 1 mM PMSF, protease and phosphatase inhibitor cocktails). Beads were boiled for 5 min in SDS-PAGE buffer (125 mM Tris-HCl, 10% glycerol, 4% SDS, 5% β-mercaptoethanol 0.005% bromophenol blue), and the supernatant was collected and analyzed by western blotting.

ERK2 Quantitation by ELISA

Cell Growth and Lysis

This was performed as described above for coimmunoprecipitation with a modified lysis buffer (20 mM Tris-HCl, 100 mM NaCl, 300 mM ammonium sulfate, 10% glycerol, 10 mM MgCl₂, 1 mM EDTA, 1 mM EGTA, 1% Triton-X, 0.25% SDS, 1 mM PMSF, protease inhibitor cocktail, phosphatase inhibitor cocktails).

ELISA

The total ERK1/2 ELISA kit (Invitrogen #KHO0081) was used according to the manufacturer's instructions.

SUPPLEMENTAL REFERENCES

- Baudin-Baillieu, A., Guillemet, E., Cullin, C., and Lacroute, F. (1997). Construction of a yeast strain deleted for the TRP1 promoter and coding region that enhances the efficiency of the polymerase chain reaction-disruption method. *Yeast* 13, 353–356.
- Bellí, G., Garí, E., Piedrafita, L., Aldea, M., and Herrero, E. (1998). An activator/repressor dual system allows tight tetracycline-regulated gene expression in budding yeast. *Nucleic Acids Res.* 26, 942–947.
- Gao, X.D., Caviston, J.P., Tcheperegine, S.E., and Bi, E. (2004). Pxl1p, a paxillin-like protein in *Saccharomyces cerevisiae*, may coordinate Cdc42p and Rho1p functions during polarized growth. *Mol. Biol. Cell* 15, 3977–3985.
- Levchenko, A., Bruck, J., and Sternberg, P.W. (2000). Scaffold proteins may biphasically affect the levels of mitogen-activated protein kinase signaling and reduce its threshold properties. *Proc. Natl. Acad. Sci. USA* 97, 5818–5823.
- Lorenz, D.R., Cantor, C., and Collins, J.J. (2009). A network biology approach to aging in yeast. *Proc. Natl. Acad. Sci. USA* 106, 1145–1150.

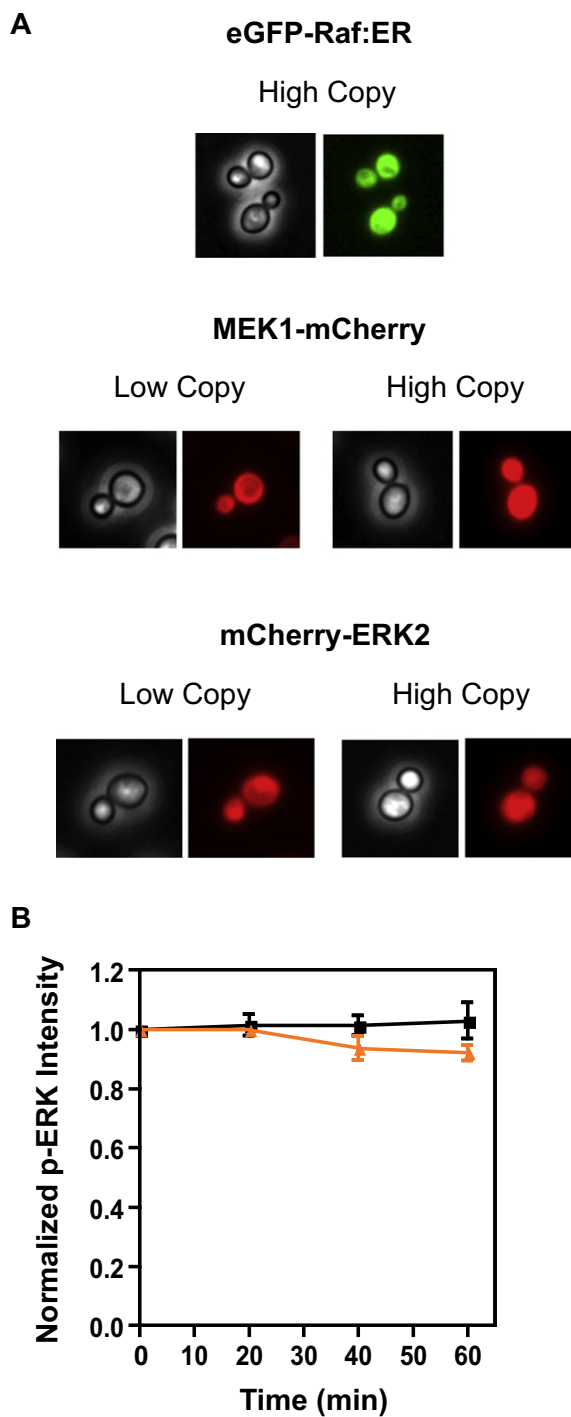


Figure S1. Component Localization and Interaction with Endogenous Phosphatases, Related to Figure 1

(A) Representative phase contrast and fluorescence microscopy images of cells expressing eGFP: Δ Raf-1:ER (Raf:ER), MEK1-mCherry, or mCherry-ERK2. Low-copy expression was from a single-integrated copy of P_{tetO7} induced with 0.5 μ g/ml aTC and high-copy expression was from episomal P_{Gal} induced with 2% galactose. Low-copy expression of Raf:ER is not shown due to the high green autofluorescence of aTC.

(B) Dephosphorylation of the basic synthetic cascade after the removal of estradiol in the presence (black) or absence (orange) of the phosphatase inhibitors pervanadate and sodium fluoride. The data represent the mean \pm SEM.

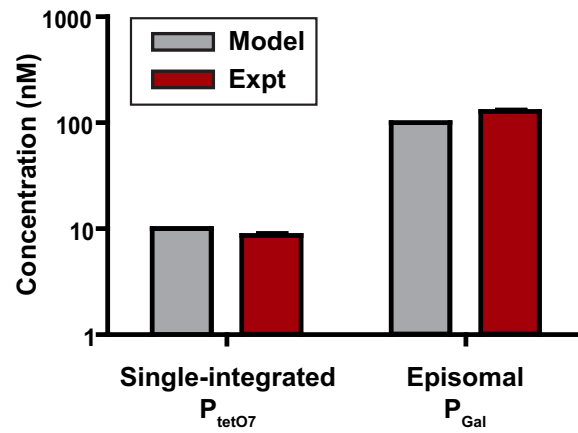


Figure S2. Total ERK2 Quantitation, Related to Figure 2

The concentration of ERK2 expressed from a single-integrated copy by P_{tetO7} induced with 0.5 $\mu\text{g/ml}$ aTC and from a high-copy episomal P_{Gal} induced with 2% galactose, determined by model predictions (gray) and quantified experimentally by ELISA (red). The data represent the mean \pm SEM.

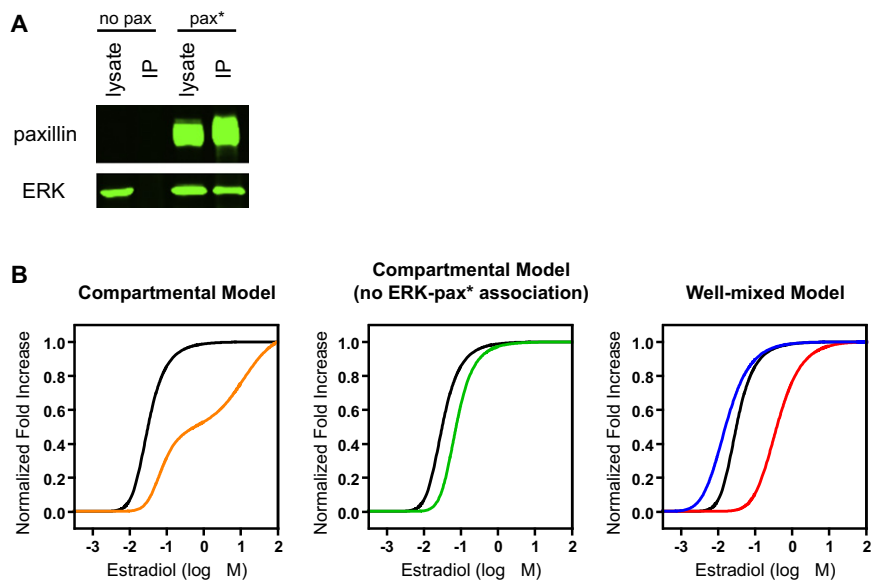


Figure S3. Coimmunoprecipitation of pax* and ERK2 and Computational pax* Models, Related to Figure 3

(A) Crude cell lysate was immunoprecipitated with antibody against paxillin and detected by Western blot using both paxillin and total ERK antibodies, demonstrating association of ERK2 and pax*.

(B) The basic cascade is shown in black on all graphs. The compartmental scaffold model was simulated assuming that ERK associates with pax* (orange; left panel) and under the constraint that ERK does not associate with pax* (green; middle panel). Representative curves of a well-mixed scaffold model are also presented (right panel). Importantly, neither the well-mixed model nor the compartmental model assuming no ERK-pax* association are capable of generating a biphasic dose-response curve, supporting our hypothesis that compartmentalization is necessary to see this behavior.

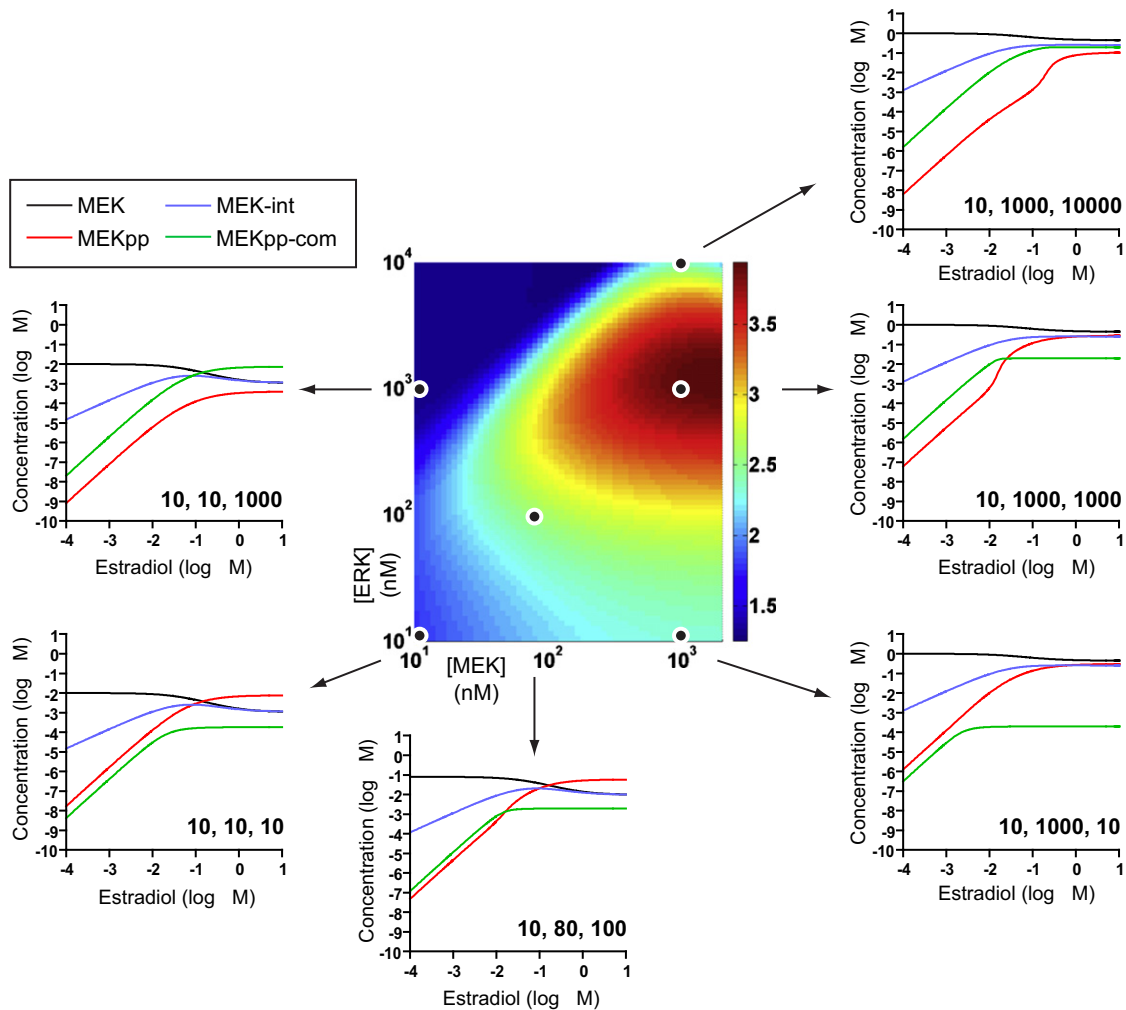


Figure S4. MEK Species as a Function of Concentration for the Dual-Step Mass Action Kinetic Model, Related to Figure 5

Specific MEK species are shown for the corresponding points on a heat map of the Hill coefficient as a function of concentration. MEK: free unphosphorylated MEK (black); MEK-int: sum of all MEK intermediates including unphosphorylated MEK bound to active Raf (MEK-Raf*), free singly phosphorylated MEK (MEKp), and singly phosphorylated MEK bound to active Raf (MEKp-Raf*) (blue); MEKpp: free active MEK (red); and MEKpp-com: sum of active MEK in complex with either unphosphorylated ERK (ERK-MEKpp) or singly phosphorylated ERK (ERKp-MEKpp) (green). Each subplot is labeled with the specific kinase concentrations in nM (Raf, MEK, ERK) used for that simulation. Ultrasensitivity is strongly dependent on the relative concentration of kinases and is low when either MEK or ERK is limited. The distribution of MEK species can be used to assess the overall fitness of a given cascade. The active species of MEK is partitioned between free (red line) and complex-bound (green line) pools and the behavior of these different populations is a function of concentration. When a cascade is MEK limited (e.g., 10,10,1000 and 10,1000,10000), the majority of active MEK is complex bound, regardless of stimulus concentration, as a large pool of ERK must be activated by a small amount of MEK. Conversely, for ERK limited systems (e.g., 10,10,10 and 10,1000,10), the majority of active MEK is free as there is much more active MEK available than is needed to maximally activate the modest quantity of ERK substrate. However, when the concentrations of MEK and ERK are well balanced (e.g., 10,80,100 and 10,1000,1000), the dose-response curves of the free-active MEK and the complex-bound MEK intersect such that the system is biased toward complex-bound MEK for low stimulus concentrations, yet becomes dominated by free MEK at high stimulus levels. The transition between these two regimes results in a sharp increase in the response of the system and leads to higher ultrasensitivity.

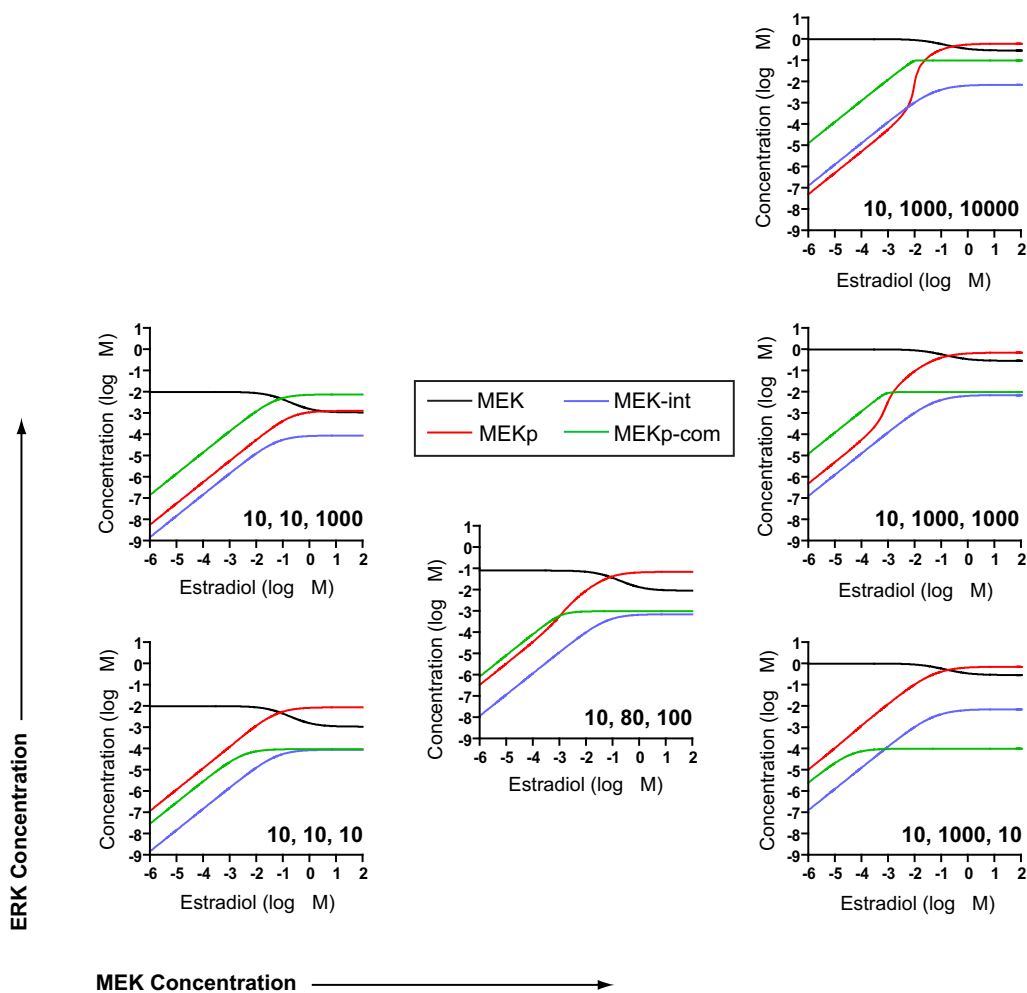


Figure S5. MEK Species as a Function of Concentration for the Single-Step Mass Action Kinetic Model, Related to Figure 5

Specific MEK species are shown for various concentrations in nM indicated on each plot (Raf, MEK and ERK concentration). MEK: free inactive MEK (black); MEK-int: inactive MEK bound to active Raf (MEK-Raf*) (blue); MEKp: free active MEK (red); and MEKp-com: active MEK bound to inactive ERK (ERK-MEKp) (green). As with the dual-step mass-action kinetic model (Figure S4 and Table S2), the ERK ultrasensitivity is low when either MEK (10,10,1000) or ERK (10,10,10 and 10,1000,10) is limited and ERK ultrasensitivity is high when the relative concentrations of MEK and ERK are well balanced (10, 80,100; 10,1000,1000 and 10,1000,10000).